Proceedings of *RAGtime 20–22, 15–19 Oct., 16–20 Sept., 19–23 Oct., 2018/2019/2020, Opava, Czech Republic*
Z. Stuchlík, G. Török and V. Karas, editors, Silesian University in Opava, 2020, pp. 287–297

287

From gappy to ringed: signatures of an accretion disk radial structure in profiles of the reflection line

Marcel Štolc,[1a] Michal Zajaček[2] and Vladimír Karas[1]

[1]Astronomical Institute of the Czech Academy of Sciences,
 Boční II 1401, CZ-14100 Prague, Czech Republic
[2]Center for Theoretical Physics, Polish Academy of Sciences,
 Al. Lotników 32/46, 02-668 Warsaw, Poland
[a]stolcml@gmail.com

ABSTRACT

The standard scenario of a geometrically thin, planar accretion disk can be violated by a number of effects that must operate in astrophysically more realistic schemes. Even within a highly simplified framework of an axially symmetric (2D), steady, Keplerian accretion, the radial structure can be different from the predictions of the classical Shakura-Sunyaev theory. In this contribution, we consider stars and stellar-mass black holes that can be embedded within the accretion disk, where they can induce the formation of gaps in the radial density profile. We focus on the theoretical profiles of a spectral line produced by reflection of the surface of both gappy accretion disk and a ring-like structure near a black hole. We describe the relativistic effects in an approximative manner. While a smooth accretion disk leads to a typical, double-horn shape with unequal wings due to Doppler boosting and an additional peak due to the lensing amplification at high inclination angle, the gaps and rings give rise to a more complex dependence which reflects the location and the radial extent of the inhomogeneities in the accretion flow.

Keywords: black holes – accretion disks – radiation

1 INTRODUCTION

Vigorous accretion of matter onto a supermassive black hole is the most essential characteristic of Active Galactic Nuclei (AGN; Peterson, 2009). While astrophysical black holes are described by only two parameters, mass M and angular momentum J (Misner et al., 1973), parameters of the gaseous flow are countless. They can span a very wide range of values depending on the AGN type, which is determined mainly by the surrounding cosmic environment. Especially the accretion rate, $\dot{M}$, and its efficiency, η, are crucial. However, also the geometry of the accretion flow plays an important role. We start our discussion by assuming hydrodynamical accretion structure, where the flow maintains a standard-type, planar, geometrically thin accretion disk (cf. Shakura and Sunyaev, 1973;

Page and Thorne, 1974), or a more luminous slim accretion disk (Abramowicz et al., 1988; Narayan and Yi, 1994)) with higher luminosity and non-negligible thickness in the vertical direction. Properties of the system are further defined by the central black hole: the Kerr metric with the outer radius of the event horizon and the spin parameter $a \equiv J/Mc^2$. Also the presence of an outflow or a magnetized jet emanating along the rotation axis will needs to be taken into account in radio loud AGN (see Boettcher et al., 2012 for a review).

We start our discussion by assuming the standard, stationary and axially symmetric accretion flow orbiting at Keplerian velocity in the equatorial plane. The continued accretion maintains a certain level of activity of the system. We neglect the effects of self-gravity of the accretion flow, which might lead to the development of density enhancements ("planets") in some locations, however, we consider the presence of a body which orbits at a certain radius in the plane and represents an embedded star, which had formed within the disk or whose trajectory became inclined into the accretion disk by the preceding orbital evolution (Collin and Zahn, 1999; Karas and Šubr, 2001). Depending on the system parameters, the star may or may not induce a radial gap in the accretion disk.

We assume that the star orbital evolution starts at a larger distance (at the grinding radius, Syer et al., 1991) which is the distance where the orbit is dragged into the disk plane. Then it proceeds gradually down to smaller radii. The time-scale of the process depends on the accretion disk parameters (esp. the accretion rate, $\dot{M}$), parameters of the star (radius $R_\star$, mass $M_\star$), and those of the central black hole. Depending on these parameters the orbital evolution is dominated by losses of orbital energy and orbital angular momentum of the star via density waves, gap formation, or gravitational waves (relevant just very close to BH; see e.g. Ward, 1986; Artymowicz, 1994; Karas and Šubr, 2001; Narayan, 2000) .

Indeed, gaps in gaseous disks are often explained by the presence of embedded bodies - stars and planets. They form due to the action of Lindblad and viscous torques (e.g. Lin and Papaloizou, 1986, and subsequent citations) and they can deepen by consuming the gas (Lubow and D'Angelo, 2006; Rosenthal et al., 2020). Vice versa, as an embedded star proceeds closer to the critical radius, it can act as a source of material for the accretion disk in the moment of its tidal disruption or partial tidal disruption (Hills, 1975; Rees, 1988).

Recent observations hint that the gap formation might be revealed via the sudden transformation of the X-ray properties of AGN (Ricci et al., 2020). These events offer a way to peer into change of the nature of radiative processes such as tidal disruption. Furthermore, Gültekin and Miller (2012) show that the theoretical study of the spectral energy distribution (SED) offers a way of accretion disk structure diagnosis, such as gaps in the inner disk in case of the black hole merger.

A gappy structure of accretion disks may actually be universal during the system evolution. This is, on one hand, related to the structure formation in the Universe, when frequent merger events during the peak of the quasar activity, led to the formation of supermassive black hole binary and triple systems. Before the black hole merger, a formation of a gap or at least a crescent in the disk is natural (Gültekin and Miller, 2012). A second scenario does not even depend on the presence of other bodies around the primary black hole. It is generally believed that accretion flows undergo transitions in basic magneto-hydrodynamic properties – the thin cold disk is located towards the outer parts of the accretion flow, while in the inner parts, hot diluted advection dominated accretion flows (ADAFs) are present (Yuan and Narayan, 2014). The ADAF part can be expanding or contracting, which leads

to the shift of the source position in the X-ray hardness–luminosity diagram ("q-shaped" or "turtle-head" diagram, Fender et al., 2004; Svoboda et al., 2017). The truncation radius where the thin disk transforms into the hot diluted flow shrinks with the increasing accretion rate $\dot{M}$ (Esin et al., 1997; Narayan and McClintock, 2008; Yuan and Narayan, 2014). Given that ADAFs have significantly lower densities than thin cold disks, they could be perceived as evolving "gaps" in the disk.

2   MODEL

Stars can get on bound orbits close to the central supermassive black hole by two dynamical channels (Mapelli and Gualandris, 2016):

(1)   *in-situ* formation, where stars form locally in a non-standard way from a denser gas,

(2)   *migration* scenario, in which stars form at larger distances and migrate inwards via a fast dynamical process.

Both processes likely contributed to the build-up of the nuclear star cluster at the center of the Milky Way, which is one of the densest stellar clusters in the Galaxy and an ideal testbed for studying stellar dynamical processes close to the supermassive black hole (Schödel et al., 2014; Alexander, 2017). In the first *in situ* scenario, stars can either form in the outer parts of an accretion disk or in the infalling molecular cloud that undergoes a disruption. In the second *migration* scenario, stars are brought to the black hole in the infalling stellar cluster. In addition, the disruption of a binary on an eccentric orbit, so-called Hills mechanism, is a special case of the migration mechanism. In the following, we use the second *migration* scenario to illustrate how a group of stars can get aligned with the accretion disk plane and subsequently perturb its structure.

The stochastic perturbations of the trajectory of a stellar cluster can cause it to wander into the Galactic centre where it becomes gravitationally bound to the supermassive black hole at its centre. The star cluster then orbits the supermassive black hole with its constituents (stars) crossing the accretion disk during each passage (e.g. Šubr and Karas, 1999; MacLeod and Lin, 2020). The repetitive intersections of stars and the accretion disk together with the drag of the accretion disk induce that the stars with non-zero inclination converge onto the orbital plane of the accretion disk. In addition, once in the orbital plane, the high-eccentric trajectories get circularized. That leads to the power-law change of the star cluster distribution (Karas and Šubr, 2001).

In the following, let us define the effective radius of a star, $R_{\text{inf}\star}$. This is a length-scale where the stellar gravitational or the magneto-hydrodynamic influence prevails over that of the black hole gravitational influence or the accretion disk total pressure (ram+thermal+magnetic pressure), respectively. The ratio of the sphere of the influence of the star and the accretion disk scale-height $\frac{R_{\text{inf}\star}}{H}$ predisposes the ability of the star to form a gap or not with the basic condition $\frac{R_{\text{inf}\star}}{H} \gtrsim 1$ and $\frac{R_{\text{inf}\star}}{H} < 1$, respectively. In the latter case, the stars get engulfed by the accretion disk gas while co-rotating with it and will eventually give rise to density waves propagating through the disk. The stellar influence radius also depends on the sense of the orbital motion. For wind-blowing stars, it is larger for stars co-rotating with the disk and smaller for stars counter-rotating. For the counter-rotating wind-blowing stars,

the stagnation radius gets smaller because of the larger relative velocity. The ratio of the stagnation radii between the co-rotating and the counter-rotating orbits can be expressed as $R_{\text{stag}}^{\text{c}}/R_{\text{stag}}^{\text{cc}} \sim \sqrt{4\zeta^2 + 1} > 1$, where $\zeta = v_{\text{K}}/c_{\text{s}}$ is the ratio of the local Keplerian velocity to the local sound speed. On the other hand, for the objects without any type of the outflow (e.g. stellar black holes), the counter-rotating orbits with respect to the accretion disk are expected to have a larger tidal Hill radius by a factor of as much as $R_{\text{H}}^{\text{cc}}/R_{\text{H}}^{\text{c}} \sim 3^{2/3} \sim 2.08$ (for circular orbits) in comparison with perturber orbits co-rotating with the disk material (Innanen, 1979; Zajaček et al., 2014). These estimates of tidal radii are based on the simple particle approximation and will be investigated in detail in our future studies.
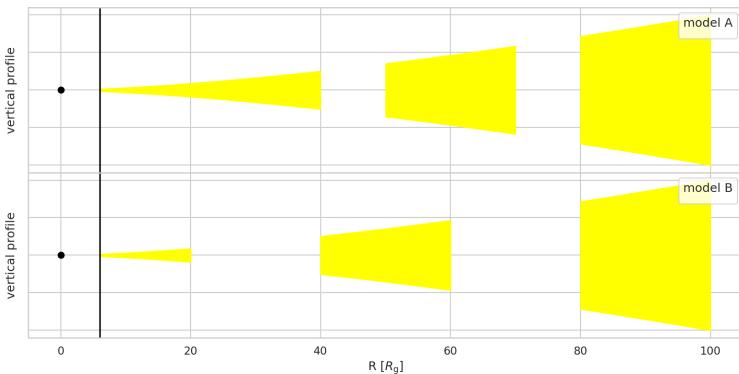

Figure 1. Two examples illustrate how we describe gaps in the model of a gappy accretion disk spectral line: model A (narrow gaps within the disk; see the top panel) in comparison with a ring-like structure in B (wide intervals separate rather narrow accretion rings; see the bottom panel). The black point marks the position of a supermassive black hole; the black vertical line is the ISCO radius.

We build upon the earlier results of Štolc et al. (2020) (in prep.), where we simulated the spectral line profiles with an accretion disk having only one gap. In our current toy model, we we allow the concurrent existence of multiple gaps. Thus, we divide our study into two scenarios – a gappy accretion disk (model A) and ring-like accretion disk (model B) based on the size of the gaps (see Figure 1). In other words, the extreme case of A would be the smooth disk, where the gaps disappear, whereas the extreme B case just corresponds to several narrow rings separated from each other (Sochora et al., 2011).

3   METHODOLOGY AND RESULTS

In our model, we assume the supermassive black hole to be of Schwarzschild type, which corresponds to the case of a vacuum metric solution outside of an object with the electric charge and the angular momentum equal to zero. We further consider the whole system to be immersed in high-energetic medium – corona. The intrinsic profile of radiation reflected on an accretion disk depends on the ratio of size of the accretion disk and the corona $\frac{R}{R_c}$

(Fabian et al., 1989). Fabian et al. (1989) show that the dependence of the intrinsic profile of the reflected radiation is $\propto \frac{1}{R^2}$ for the ratio $\frac{R}{R_c} \approx 1$ and $\propto \frac{1}{R^3}$ for the ratio $\frac{R}{R_c} > 1$.

Calculation of the monochromatic flux of radiation reflected on an accretion disk follows from the general definition (e.g. Hubený and Mihalas, 2014),

$$F_\nu^i = \int I_\nu(n_x, n_y, n_z) n^i \mathrm{d}\Omega, \ i = 1, 2, 3 \tag{1}$$

integrating over all solid angles. The matter distribution in our model corresponds to the standard Shakura-Sunyaev thin disk scheme (cf. Shakura and Sunyaev, 1973; Page and Thorne, 1974). Adopting the axial symmetry of the system ($\partial_\varphi = 0$) the eq. (1) reads as

$$F_\nu \approx \int I_\nu \, \mathrm{d}S, \ \mathrm{d}S = R \, \mathrm{d}R \, \mathrm{d}\varphi. \tag{2}$$

To get observed values of the monochromatic flux of radiation we have to use the Liouville's theorem that is referencing the special relativistic relation between *observed* and *emitted* intensity and frequency as

$$\frac{I_{\text{observed}}}{I_{\text{emitted}}} = \frac{\nu_{\text{observed}}^3}{\nu_{\text{emitted}}^3}. \tag{3}$$

The ratio of *observed* and *emitted* frequency defines the gravitational redshift

$$g = \frac{\nu_{\text{observed}}}{\nu_{\text{emitted}}}. \tag{4}$$

Combining the eq. (2), (3) and (4) we get the expression for the observed monochromatic flux of radiation as

$$F_{\text{observed}} \approx \int \frac{\nu_{\text{observed}}^3}{\nu_{\text{emitted}}^3} I_{\text{emitted}} \mathrm{d}S = \int g^3 I_{\text{emitted}} \, \mathrm{d}S, \ \mathrm{d}S = R \, \mathrm{d}R \, \mathrm{d}\varphi. \tag{5}$$

Assuming the supermassive black hole in our simulations to be a Schwarzschild black hole we use the redshift factor accounting not only for the special relativistic effect but for the gravitational light-bending as well. The redshift factor then reads as (Pecháček et al., 2005)

$$g(R, \varphi, I) = \frac{\sqrt{R(R-3)}}{R + \sin(\varphi)\sin(I)\sqrt{R - 2 + 4(1 + \cos(\varphi)\sin(I))^{-1}}} \tag{6}$$

with R, φ and I as radial co-ordinate, azimuthal co-ordinate and inclination respectively. In order to observe both special and general relativistic effects of the simulated spectral line profiles more clearly we limit our calculations in sense of radial extent of the accretion disk, i.e. the range of radial co-ordinate is ($6R_g$, $100 \, R_g$).

The following plots examine the background-subtracted spectral features, so the underlying continuum is neglected. Figures 2–7 show the comparison of the spectral line profile for both models A and B (with gaps) with the intrinsic profile of reflected radiation as $\propto \frac{1}{R^2}$ and $\propto \frac{1}{R^3}$ from the entire disk (without gaps, i.e., unperturbed). Red dashed vertical line marks the intrinsic frequency.

◀◀ ◀ ▶ ▶▶ ↩ ↪ ? ▢ ■ ✖

The spectral line profiles are quite narrow which is caused due to the lower value of inclination as 35 deg (see Figures 2–3). We observe the decrease of the radiation flux of the spectral line in the model B compared to the model A. We can also notice that the number of peaks in the spectral line of the perturbed accretion disk is three times more that of the case involving the unperturbed accretion disc.
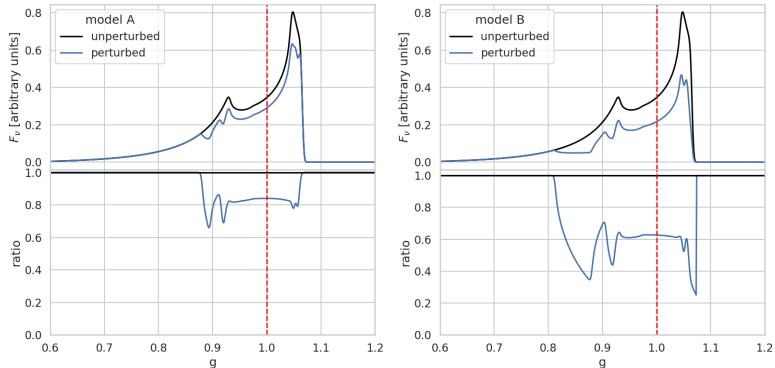

Figure 2. Comparison of spectral line profiles for model A (left panel) and model B (right panel) with intrinsic intensity $I_\nu \propto \frac{1}{R^2}$. The view angle is 35 deg.
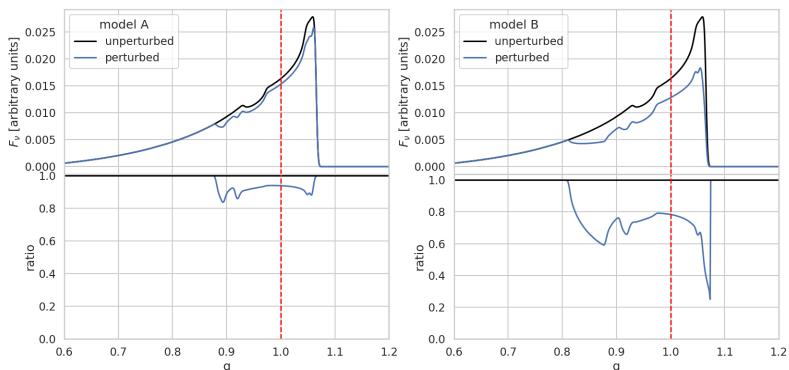
Figure 3. The same as in the previous figure but for $I_\nu \propto \frac{1}{R^3}$.

Changing the value of the inclination to 60 deg and 85 deg (see Figures 4–5 and Figures 6–7, respectively) the spectral line profiles get more stretched. Hence we observe the decrease of the of the radiation flux in the spectral line of model B compared to model A more

clearly as it spans across bigger region of *observed* frequencies. The number and positions of the spectral line peaks are more distinguishable as well.
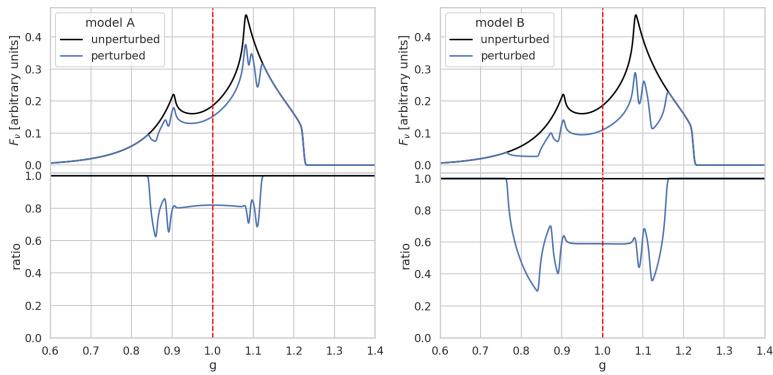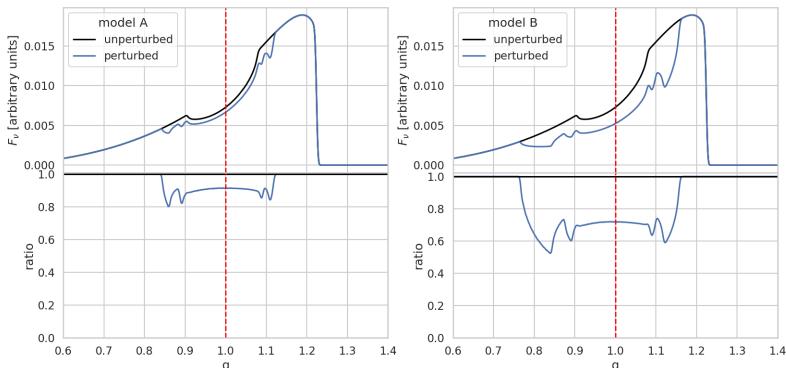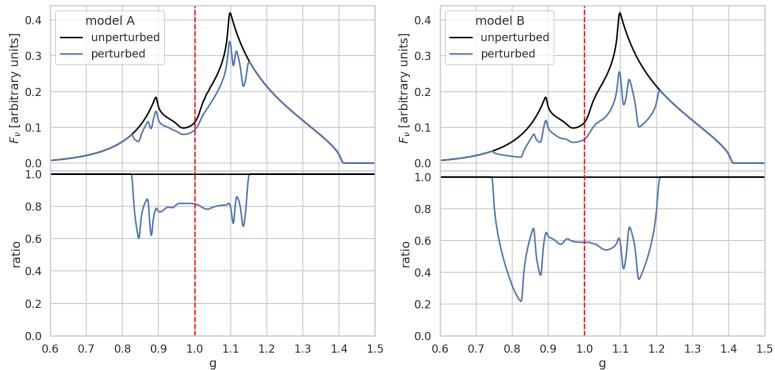

Figure 4. Comparison of spectral line profiles for model A (left panel) and model B (right panel) with intrinsic intensity $I_\nu \propto \frac{1}{R^2}$. The view angle is 60 deg.

Figure 5. The same as in the previous figure but for $I_\nu \propto \frac{1}{R^3}$.

Figure 6. Comparison of spectral line profiles for model A (left panel) and model B (right panel) with intrinsic intensity $I_\nu \propto \frac{1}{R^2}$. The view angle is 85 deg.
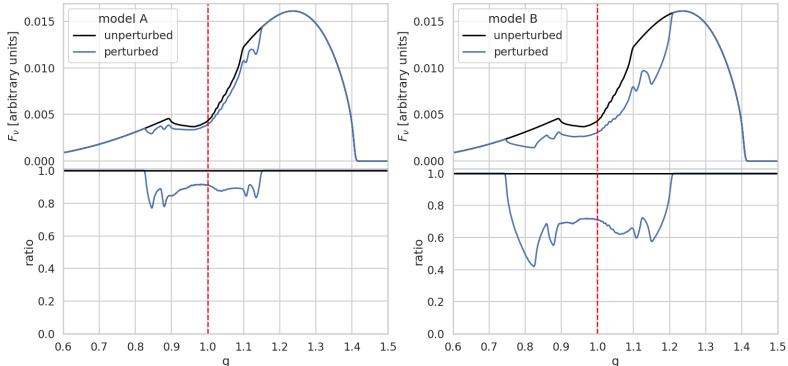

Figure 7. The same as in the previous figure but for $I_\nu \propto \frac{1}{R^3}$.

The spectral line profiles for the model B show overall less radiation flux than the spectral line profiles for the model A, independent on the intrinsic radiation intensity of the reflected radiation. That is to be expected as the area of reflection medium in model B is smaller than the area of reflection medium in model A. The number of peaks in both model A and model B equals to 6. That is a direct result of superposition of 3 spectral line profiles coming from the 3 individual "sub-disks" of the former unperturbed accretion disk structure.

4 DISCUSSION AND CONCLUSIONS

Our plots of the model reflection line show how the growing number of gaps in the accretion disk, their radial position and width lead to a growing complexity of the spectral profile, namely, the number of peaks compared to an unperturbed case. The latter exhibits just two peaks of the classical double-horn shape depending on the observer's view angle (Karas et al., 1992). To be more specific in our examples, we expect that number N of gaps, will result in spectral line profile with $(2N + 2)$ peaks (in the above given example, e.g., $N = 2$ translates to 6 peaks). Changing from the model A to B we clearly observe this developing spectral feature together with the decrease in the radiation flux.

The model A could correspond to a binary star being trapped by the supermassive black hole potential. After the component separation of the binary system they both subsequently induce gaps, given the condition $\frac{R_{\inf \star}}{H} \gtrsim 1$ holds for each one. The accretion disks on the verge of collapse due thermal or viscous perturbations tend to form rings and dissolve (e.g. Frank et al., 2002). This rather short stage transition would be in agreement with the model B that we propose.

We defer the study of astrophysically realistic interpretation of gap sizes together with respective timescales (e.g. Takeuchi et al., 1996) which will require taking into account the gravitational sphere of influence of a smaller body in face of perturbations from a more massive one, as governed by the Hill or Bondi-Hoyle-Lyttleton radii, respectively. Further analysis will have to consider the interaction of both the stellar wind and the magnetosphere with the accretion disk's gas (e.g., Zajaček et al., 2015, 2016), so the radius of sphere of influence of a star should then lead to the formation of relatively wide gaps.

ACKNOWLEDGEMENTS

REFERENCES

Abramowicz, M. A., Czerny, B., Lasota, J. P. and Szuszkiewicz, E. (1988), Slim Accretion Disks, *ApJ*, **332**, p. 646.

Alexander, T. (2017), Stellar Dynamics and Stellar Phenomena Near a Massive Black Hole, *ARA&A*, **55**(1), pp. 17–57, arXiv: 1701.04762.

Artymowicz, P. (1994), Orbital Evolution of Bodies Crossing Disks Due to Density and Bending Wave Excitation, *ApJ*, **423**, p. 581.

Boettcher, M., Harris, D. E. and Krawczynski, H. (2012), *Relativistic Jets from Active Galactic Nuclei*.

Collin, S. and Zahn, J.-P. (1999), Star formation and evolution in accretion disks around massive black holes., *A&A*, **344**, pp. 433–449.

Esin, A. A., McClintock, J. E. and Narayan, R. (1997), Advection-Dominated Accretion and the Spectral States of Black Hole X-Ray Binaries: Application to Nova Muscae 1991, *ApJ*, **489**(2), pp. 865–889, arXiv: `astro-ph/9705237`.

Fabian, A. C., Rees, M. J., Stella, L. and White, N. E. (1989), X-ray fluorescence from the inner disc in Cygnus X-1., *MNRAS*, **238**, pp. 729–736.

Fender, R. P., Belloni, T. M. and Gallo, E. (2004), Towards a unified model for black hole X-ray binary jets, *MNRAS*, **355**(4), pp. 1105–1118, arXiv: `astro-ph/0409360`.

Frank, J., King, A. and Raine, D. (2002), Accretion Power in Astrophysics, *Cambridge University Press; 3 edition*, pp. 80–84.

Gültekin, K. and Miller, J. M. (2012), Observable Consequences of Merger-driven Gaps and Holes in Black Hole Accretion Disks, *ApJ*, **761**(2), 90, arXiv: `1207.0296`.

Hills, J. G. (1975), Possible power source of Seyfert galaxies and QSOs, *Nature*, **254**, pp. 295–298.

Hubený, I. and Mihalas, D. (2014), *Theory of Stellar Atmospheres*, ISBN ISBN9781400852734.

Innanen, K. A. (1979), The limiting radii of direct and retrograde satellite orbits, with applications to the solar system and to stellar systems., *AJ*, **84**, pp. 960–963.

Karas, V., Vokrouhlický, D. and Polnarev, A. G. (1992), In the vicinity of a rotating black hole: a fast numerical code for computing observational effects., *MNRAS*, **259**, pp. 569–575.

Karas, V. and Šubr, L. (2001), Orbital decay of satellites crossing an accretion disc, *A&A*, **376**, pp. 686–696, arXiv: `astro-ph/0107232`.

Lin, D. N. C. and Papaloizou, J. (1986), On the Tidal Interaction between Protoplanets and the Protoplanetary Disk. III. Orbital Migration of Protoplanets, *ApJ*, **309**, p. 846.

Lubow, S. H. and D'Angelo, G. (2006), Gas Flow across Gaps in Protoplanetary Disks, *ApJ*, **641**(1), pp. 526–533, arXiv: `astro-ph/0512292`.

MacLeod, M. and Lin, D. N. C. (2020), The Effect of Star-Disk Interactions on Highly Eccentric Stellar Orbits in Active Galactic Nuclei: A Disk Loss Cone and Implications for Stellar Tidal Disruption Events, *ApJ*, **889**(2), 94, arXiv: `1909.09645`.

Mapelli, M. and Gualandris, A. (2016), *Star Formation and Dynamics in the Galactic Centre*, volume 905, p. 205.

Misner, C. W., Thorne, K. S. and Wheeler, J. A. (1973), *Gravitation (San Francisco: W.H. Freeman and Co)*.

Narayan, R. (2000), Hydrodynamic Drag on a Compact Star Orbiting a Supermassive Black Hole, *ApJ*, **536**(2), pp. 663–667, arXiv: `astro-ph/9907328`.

Narayan, R. and McClintock, J. E. (2008), Advection-dominated accretion and the black hole event horizon, *NewAR*, **51**(10-12), pp. 733–751, arXiv: `0803.0322`.

Narayan, R. and Yi, I. (1994), Advection-dominated Accretion: A Self-similar Solution, *ApJL*, **428**, p. L13, arXiv: `astro-ph/9403052`.

Page, D. N. and Thorne, K. S. (1974), Disk-Accretion onto a Black Hole. Time-Averaged Structure of Accretion Disk, *ApJ*, **191**, pp. 499–506.

Pecháček, T., Dovčiak, M. and Karas, V. (2005), The relativistic shift of spectral lines from black-hole accretion discs, pp. 137–141.

Peterson, B. M. (2009), *Active galactic nuclei (Cambridge Univ. Press: Cambridge)*, p. 138.

Rees, M. J. (1988), Tidal disruption of stars by black holes of 10^6-10^8 solar masses in nearby galaxies, *Nature*, **333**(6173), pp. 523–528.

Ricci, C., Kara, E., Loewenstein, M., Trakhtenbrot, B., Arcavi, I., Remillard, R., Fabian, A. C., Gendreau, K. C., Arzoumanian, Z., Li, R., Ho, L. C., MacLeod, C. L., Cackett, E., Altamirano, D., Gand hi, P., Kosec, P., Pasham, D., Steiner, J. and Chan, C. H. (2020), The Destruction and

Recreation of the X-Ray Corona in a Changing-look Active Galactic Nucleus, *ApJL*, **898**(1), p. L1.

Rosenthal, M. M., Chiang, E. I., Ginzburg, S. and Murray-Clay, R. A. (2020), How consumption and repulsion set planetary gap depths and the final masses of gas giants, *MNRAS*, **498**(2), pp. 2054–2067, arXiv: 2004.13720.

Schödel, R., Feldmeier, A., Neumayer, N., Meyer, L. and Yelda, S. (2014), The nuclear cluster of the Milky Way: our primary testbed for the interaction of a dense star cluster with a massive black hole, *Classical and Quantum Gravity*, **31**(24), 244007, arXiv: 1411.4504.

Shakura, N. I. and Sunyaev, R. A. (1973), Reprint of 1973A&A....24..337S. Black holes in binary systems. Observational appearance., *A&A*, **500**, pp. 33–51.

Sochora, V., Karas, V., Svoboda, J. and Dovčiak, M. (2011), Black hole accretion rings revealed by future X-ray spectroscopy, *MNRAS*, **418**(1), pp. 276–283, arXiv: 1108.0545.

Svoboda, J., Guainazzi, M. and Merloni, A. (2017), AGN spectral states from simultaneous UV and X-ray observations by XMM-Newton, *A&A*, **603**, A127, arXiv: 1704.07268.

Syer, D., Clarke, C. J. and Rees, M. J. (1991), Star-disc interactions near a massive black hole, *MNRAS*, **250**, pp. 505–512.

Takeuchi, T., Miyama, S. M. and Lin, D. N. C. (1996), Gap Formation in Protoplanetary Disks, *ApJ*, **460**, p. 832.

Šubr, L. and Karas, V. (1999), An orbiter crossing an accretion disc, *A&A*, **352**, pp. 452–458, arXiv: astro-ph/9910401.

Ward, W. R. (1986), Density waves in the solar nebula: Diffential Lindblad torque, *Icar*, **67**(1), pp. 164–180.

Yuan, F. and Narayan, R. (2014), Hot Accretion Flows Around Black Holes, *ARA&A*, **52**, pp. 529–588, arXiv: 1401.0586.

Zajaček, M., Eckart, A., Karas, V., Kunneriath, D., Shahzamanian, B., Sabha, N., Mužić, K. and Valencia-S., M. (2016), Effect of an isotropic outflow from the Galactic Centre on the bow-shock evolution along the orbit, *MNRAS*, **455**(2), pp. 1257–1274, arXiv: 1510.02285.

Zajaček, M., Karas, V. and Eckart, A. (2014), Dust-enshrouded star near supermassive black hole: predictions for high-eccentricity passages near low-luminosity galactic nuclei, *A&A*, **565**, A17, arXiv: 1403.5792.

Zajaček, M., Karas, V. and Kunneriath, D. (2015), Galactic Center Minispiral: Interaction Modes of Neutron Stars, *Acta Polytechnica*, **55**(3), pp. 203–214, arXiv: 1507.00706.